

# The Relativistic Cornell-type Mechanism of Exotic Scalar Resonances

A.M. Badalian,<sup>\*</sup> M.S. Lukashov,<sup>†</sup> and Yu.A. Simonov<sup>‡</sup>  
*NRC “Kurchatov Institute” – ITEP, B. Chermushkinskaya 25, Moscow, 117259, Russia*  
(Dated: January 22, 2020)

Theory of the coupled  $q\bar{q}$  and the  $\varphi\varphi(\pi - \pi, K\bar{K}, \pi K, \dots)$  scalar channels is formulated, taking into account the ground and radial excited  $q\bar{q}$  poles. The basic role is shown to be played by the transition coefficients  $k^{(I)}(q\bar{q}, |\varphi\varphi)$ , which are calculated using the quark-chiral Lagrangian without free parameters. The resulting method, called the pole projection mechanism (PPM), ensures 1) one resonance for each  $\varphi\varphi$  channel from the basic  $q\bar{q}$  pole, e.g.  $f_0(500)$  in  $\pi\pi$  and  $f_0(980)$  in  $K\bar{K}$ , from the  $n\bar{n}$  pole around 1 GeV; 2) strong pole shift down for special  $(\pi\pi, \pi K)$  channels due to large transition coefficients  $k^{(I)}$ . The parameters of the obtained complex poles are in reasonable agreement with the experimental resonances  $f_0(500)$ ,  $f_0(980)$ ,  $a_0(980)$ ,  $a_0(1450)$ ,  $K_0^*(700)$ ,  $K_0^*(1430)$ ,  $f_0(1370)$ ,  $f_0(1710)$ .

PACS numbers:

## I. INTRODUCTION

The QCD theory of hadrons has very developed resources to treat hadron properties and by now explained a majority of observed hadrons [1]. Nevertheless, there exist hadronic objects, considered as non-standard or extra states, with the properties (e.g. the masses and widths) strongly different from theoretical predictions [2], and most of them refer to light scalar mesons, such as  $f_0(500)$ ,  $f_0(980)$ ,  $a_0(980)$ ,  $K_0^*(700)$ . They can hardly be associated with the lowest conventional  $q\bar{q}$  scalars for several reasons: a) their masses are strongly displaced as compared to expected  $q\bar{q}$  masses; b) in some cases two observed scalar resonances can be identified with one  $q\bar{q}$  state with the same quantum numbers.

This situation is well described by Nils Törnqvist in 1995 [3] “Our present understanding of the light meson mass spectrum is in a deplorable state... This is mainly because of the fact that... “QCD inspired quark models” fail so dramatically for scalar mesons...” Nowadays, 25 years later these words hold true, probably, even more spectacularly. Nevertheless continuous efforts of the physical community have brought a large amount of information about the properties of the scalars, their decays, and production (see [4–10] for reviews and analysis, and [11–13] for most recent reviews). Theoretical approaches to the scalar spectrum include the tetraquark model [14], the chiral model [15], the molecular model [16], the QCD sum rules [17], and lattice calculations [18]. On another hand one can use a simple parametrization of the  $q\bar{q}$  to the meson-meson channel transition amplitude [19],

---

<sup>\*</sup>Electronic address: badalian@itep.ru

<sup>†</sup>Electronic address: m.s.lukashov@gmail.com

<sup>‡</sup>Electronic address: simonov@itep.ru

which gives a reasonable behaviour of the scalar amplitude. An important approach to physics of the scalar resonances is the use of the dispersive and analytic methods for the analysis of the scalar meson-meson amplitudes [15], [20–26]. Despite of all efforts and large amount of information the main two problems, underlined above, are not yet resolved and in the PDG summary Table 2 [1] the lowest scalar resonances are identified with  $f_0(1370)$  for  $I = 0$  and  $a_0(1450)$  for  $I = 1$ , implying that the lowest  $1^3P_0 q\bar{q}$  pole is around (1.4-1.5) GeV, which contradicts numerous calculations in relativistic models [27–30].

The present paper, as well as the previous one [31], is aimed at the theoretical solution of the scalar meson problem and for that we shall use the method, similar to the non-relativistic Cornell coupled-channel mechanism [32], developed for heavy mesons, where the pure charmonium states  $c\bar{c}$  transform into the  $D\bar{D}$  states and back many times, leading to the displacement of resulting combined resonances. This transformation occurs via creation of a pair of light quarks and numerically is of the order or less than 50 MeV. Later on these authors have studied displaced resonances in charmonium quantitatively [33], and one of the present authors (Yu.S. together with colleagues) used the Cornell formalism to study both charmonium and bottomonium systems [34].

The general theory of channel-coupled (CC) resonances was given in [35] in a general form, not assuming pole structures in any channel, while the CC resonance can occur, as in the case of the  $\Upsilon(nS)\pi$  system coupled to  $BB^*$  or  $B^*B^*$  (see last ref. in [34]). Below we are specifically interested in the  $q\bar{q}$  poles found in relativistic path-integral formalism, coupled to a pair of chiral mesons.

One of the basic points of this method is derivation of the transition elements between the  $q\bar{q}$  and meson-meson systems, and below we use, as in [31], the quark-chiral Lagrangian [36–39], which establishes all chiral relations, known in standard chiral theory, like GMOR relations [40], but also allows to calculate the chiral decay constants,  $f_\pi, f_K, \dots$  [42]. It also correctly predicts behaviour of the chiral constants in magnetic field, where the standard chiral theory fails [41]. Our purpose in this paper is to define the exact  $q\bar{q}$  poles using the detailed relativistic theory (see [28, 30] and refs. therein) and establish explicit relations between the known  $^3P_0 q\bar{q}$  state characteristics and resulting new resonance pole parameters, which will be called the Pole Projection Mechanism (PPM). In the framework of PPM, as shown in [31], a single  $q\bar{q}$  pole can create two (several) projected resonances, one for each meson-meson channel, coupled to a given  $q\bar{q}$  channel. This mechanism was applied in the case of the  $f_0(500)$  and  $f_0(980)$  resonances [31], when from the original ( $q\bar{q}$ ) pole at  $M_1 = 1.05$  GeV two resonances,  $f_0(500)$  and  $f_0(980)$ , are created. In this way

both properties a), b) were demonstrated, since  $f_0(500)$  occurs due to  $\pi\pi$  channel coupling to the  $q\bar{q}$  initial state with the mass  $M_1$ , while  $f_0(980)$  is due to the  $K\bar{K} - q\bar{q}$  channel coupling. Simultaneously in the case with the isospin  $I = 1$  and the initial mass  $M_1$  the  $q\bar{q}$ - pole is coupled to both channels,  $\pi\eta$  and  $K\bar{K}$ , and produces two close-by resonances near 1 GeV, which can be associated with  $a_0(980)$ . As shown in [31], in the PPM there exists the only variable parameter – the spatial radius  $\lambda$  of the quark-meson transition amplitude, denoted as  $k^{(I)}(q\bar{q}, \varphi\varphi)$ .

The spatial radius  $\lambda$  enters in the quark chiral Lagrangian [36–39] as a mass parameter  $M(\lambda) = \sigma\lambda$  and is fixed in the case of  $\pi, K$  mesons by the calculation of  $f_\pi, f_K$  [41], which yields  $\lambda = 0.83 \text{ GeV}^{-1}$ . In the  $q\bar{q} - \varphi\varphi$  transition case we calculate for the first time dependence of the coefficient  $k^{(I)}(q\bar{q}, \varphi\varphi)$  on  $\lambda$  and find a stable maximum at  $\lambda = \lambda_0$  in the region ( $1 \leq \lambda_0 \leq 1.5$ )  $\text{GeV}^{-1}$ , which is taken as a basic point of our method, yielding the fixed value of  $k^{(I)}(\lambda_0)$  and the fixed  $\lambda = \lambda_0$ .

In the present paper we further extend the PPM theory to include the radial excitations of the  $q\bar{q}$  states and find the resulting scalar resonances. To this end we consider the  $n\bar{n}, n\bar{s}, s\bar{s}$  states with  $n_r = 0, 1$  and  $I = 0, 1/2, 1$ , and show that the inclusion of the radial excited  $q\bar{q}$  pole makes the PPM even more pronounced, when the lower pole, coupled with the meson-meson channels, has large shift down, while the second higher pole has much smaller shift. In this way we demonstrate the important visible feature of the scalar resonances: the lowest  $n_r = 0$  poles are much strongly shifted as compared to the  $n_r = 1$  poles.

To calculate the resulting shifted poles we need 1) the transition coefficients  $k^{(I)}(\lambda_0)$ , discussed above; 2) the  $q\bar{q}$  pole masses  $M_1, M_2$  computed in the framework of relativistic path integral Green's functions [43], and 3) the free  $\varphi\varphi$  Green's functions  $G_{\varphi\varphi}(E, \lambda_0)$ , defined with the spatial distance  $\lambda_0$  between the in and out  $\varphi\varphi$  states. As a result, we find the complex energy poles, corresponding to observed resonances  $f_0(500), f_0(980), f_0(1370), f_0(1500), a_0(980), a_0(1450), K_0^*(700), K_0^*(1430), f_0(1710)$ .

The plan of the paper is as follows. In section 2 we present the details of the PPM formalism of [31] in the case of the  $I = 0, 1/2, 1; J^P = 0^+$  channels, and in section 3 we analyse the dynamics of our theory and calculate the resulting positions of the resonances. The inclusion of radial excited  $q\bar{q}$  states and calculation of the resulting scalar resonances is done in section 4. Section 5 is devoted to the discussion of results and possible future developments of our approach.

## II. THE QUARK-CHIRAL DYNAMICS IN THE $(q\bar{q})$ -(MESON-MESON) CHANNEL

The main element of the Cornell formalism [32] is the expression for the total quark-meson Green's function (resolvent)  $\mathcal{G}(E)$  via  $q\bar{q}$  resolvent  $G_{q\bar{q}}$  and meson-meson resolvent  $G_{\varphi\varphi}$ ,

$$\mathcal{G}(E) = \frac{A}{1 - V_{q\varphi}G_{\varphi\varphi}(E)V_{\varphi q}G_{q\bar{q}}(E)}, \quad (1)$$

so that the resonance energies are to be found from the equation

$$VG_{\varphi\varphi}(E)VG_{q\bar{q}}(E) = 1, \quad (2)$$

where the main point is the transition element  $V_{q\varphi} = V_{\varphi q}^+$ .

In [32, 33] it was shown how the channel coupling in the system affects the charmonium poles. Later on, this formalism has acquired specific features, necessary to explain the poles in the heavy-quark systems, e.g. in  $X(3872)$  [34], where the original  $2^3P_1$  pole of the  $c\bar{c}$  system is strongly shifted due to transitions of  $c\bar{c}(2^3P_1)$  into  $D\bar{D}^*$  meson-meson state and back, which finally provides a pole at the  $D\bar{D}^*$  threshold. Actually the equation for the position of the new quark-meson pole has similar forms: nonrelativistic in [32–34] and relativistic in the new formulations for the scalars in [31]:  $G_{\varphi\varphi}(E)\Gamma G_{q\bar{q}}(E)\Gamma = 1$ , where  $\Gamma$  is the  $q\bar{q} - \varphi\varphi$  transition vertex, and in [31] it was found that for the chiral  $\varphi\varphi$  mesons  $\Gamma$  is large.

Note, that one could call  $X(3872)$  as the  $D\bar{D}^*$  resonance, but at the same time it can be considered as the shifted  $c\bar{c}$  resonance, implying that it is the combined  $c\bar{c} - D\bar{D}^*$  phenomenon, or the  $c\bar{c}$  pole projected on the  $D\bar{D}^*$  channel.

At this point one does not still expect that one  $c\bar{c}$  pole can interact with several  $(D\bar{D}, D\bar{D}^*, D^*\bar{D}^*)$  states and can produce more than one resonance. In the heavy quarkonia case the resulting pole shifts are of the order of  $\sim 50$  MeV, if the meson-meson thresholds are nearby the original  $Q\bar{Q}$  poles, whereas in the general case the situation can be different and, as shown in [31], in light mesons the pole shifts can reach 500 MeV. At this point it is important to stress the general features of the PPM method, when the original  $(q\bar{q})$  pole is projected into the meson-meson pole due to interaction between the  $q\bar{q}$  and chiral meson-meson channels implying a strong but meson-dependent coupling. As a result, one  $q\bar{q}$  pole can be projected into several meson-meson poles, associated with the corresponding meson-meson thresholds. As it was shown in [31], this happens in the case of the  $f_0(500)$  (the  $\pi\pi$  channel) and the  $f_0(980)$  (the  $K\bar{K}$  plus coupled  $\pi\pi$ ), which are both produced by the  $n\bar{n}(1^3P_0)$  pole at around 1 GeV. These features create a completely new

picture of possible “extra poles”, generated by the regular  $q\bar{q}$  poles in QCD, not connected to any molecular or tetraquark mechanisms. Note, that the PPM can easily be extended to the three-meson case  $(m_1, m_2, m_3)$ , coupled to the  $q\bar{q}$  pole, as it occurs in the cases with the isospin  $I = 1$ ,  $J = 1, 2$ , namely, the  $a_1(1P), a_2(1P)$  cases, which will be discussed elsewhere.

Below we shall present the PPM, which can explain the appearance of a new pole for each new meson-meson combination, starting with one original  $q\bar{q}$  pole, as it was done in the  $f_0(500), f_0(980)$  case. We start with the basic element of the PPM formalism in the case of chiral mesons – the quark-chiral Lagrangian, or Chiral Confining Lagrangian (CCL), introduced in [36–38] and extended recently in [39]. This Lagrangian is a generalization of the standard chiral theory, which takes into account not only chiral meson but also quark-antiquark d.o.f. The latter are necessary to calculate the meson coupling constants  $(f_\pi, f_K, \dots)$  [41], to write the correct Green’s functions for chiral mesons, and also to calculate the higher  $O(p^4, p^6)$  terms of chiral perturbation theory (see [39]). Moreover, the magnetic field dependent constants of chiral mesons  $(f_\pi, f_K, m_\pi, \langle q\bar{q} \rangle)$  are obtained correctly in the CCL [42], while the results of the standard CPTTh (without  $q\bar{q}$  d.o.f.) disagree with numerical calculations. Otherwise all known relations, like GMOR [40], can be derived from CCL as in the standard chiral theory.

The CCL has the form

$$L_{ECCL} = -N_c \text{tr} \log(\hat{\partial} + \hat{m} + s_0 + \hat{s} + M\hat{U}), \quad (3)$$

where  $\hat{U}$  is the standard chiral operator,

$$\hat{U} = \exp(i\gamma_5 \hat{\varphi}), \quad \hat{\varphi} = \frac{\varphi_a \lambda_a}{f_a}, \quad (4)$$

$$\hat{\varphi} = \sqrt{2} \begin{pmatrix} \frac{1}{f_\pi} \left( \frac{\eta}{\sqrt{6}} + \frac{\pi^0}{\sqrt{2}} \right), & \frac{\pi^+}{f_\pi}, & \frac{K^+}{f_K} \\ \frac{\pi^-}{f_\pi}, & \left( \frac{\eta}{\sqrt{6}} - \frac{\pi^0}{\sqrt{2}} \right) \frac{1}{f_\pi}, & \frac{K^0}{f_{K^0}} \\ \frac{K^-}{f_K}, & \frac{\bar{K}^0}{f_{K^0}}, & -\frac{2\eta}{\sqrt{6}f_\pi} \end{pmatrix}. \quad (5)$$

Here  $M$  is the  $q\bar{q}$  interaction term,  $M = \sigma r$ , in the case, when chiral operators are not present, i.e. everywhere in the  $q\bar{q}$  loop, except for the vertex, where chiral mesons of  $\hat{U}$  are emitted. In the last case, i.e. in the  $\pi$ , or the  $K$  emission vertex, the value of  $M$  is fixed at  $M(\lambda) = 0.15$  GeV, which corresponds to  $\lambda \cong 0.2$  fm – the fundamental length of the vacuum, known from the Field Correlator Method (FCM) [44]. The latter value of 0.15 GeV is exactly the one, which gives correctly

the pion and the kaon decay constants, calculated in the framework of the CCL. From [42] one has

$$\sqrt{2}f_\pi = 138 \text{ MeV}, \sqrt{2}f_K = 165 \text{ MeV},$$

which can be compared with experimental values [1]

$$\sqrt{2}f_\pi = 130.7 \pm 0.1 \pm 0.36 \text{ MeV}, \sqrt{2}f_K = 159.8 \pm 1.4 \pm 0.44 \text{ MeV}.$$

Note that  $M(\lambda)$  is the only parameter of the CCL, in addition to quark masses. The main idea of the quark-chiral approach [35–39] is that the scalar confining operator  $M(\lambda)$ , violating chiral symmetry, is augmented by the chiral operator  $U(\hat{\varphi})$ , which can emit any number of chiral mesons at the vertex of the  $q\bar{q}$  operator.

Correspondingly, one can introduce the chiral-free  $q\bar{q}$  Green's function from Eq. (3) with  $U = 1$ , which we call  $G_{q\bar{q}}$  (see Fig.1), the free meson-meson Green's function  $G_{\varphi\varphi}$ , (see Fig.2), and the transition element from  $q\bar{q}$  to the  $\varphi\varphi$  system, which is obtained from the CCL, Eq. (3), as shown in [31], see Fig.3.

$$\Delta L = -N_c \text{tr} \Lambda s \Lambda M(\lambda) \frac{\hat{\varphi}^2}{2}. \quad (6)$$

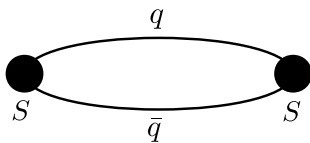


FIG. 1: The scalar  $q\bar{q}$  Green's function  $G_{q\bar{q}}$

Here  $s$  is the external current, e.g. for the  $I = 0$ , the  $f_0(500)$ ,  $f_0(980)$  cases it is equal to 1, while  $\Lambda$  is the quark propagator,  $\Lambda = (\hat{\partial} + m_q + M)^{-1}$ .

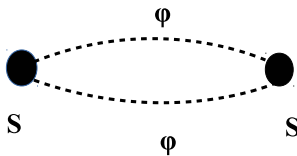


FIG. 2: The scalar  $\varphi\varphi$  Green's function  $G_{\varphi\varphi}$

The structure of the transition operator,  $M\frac{\hat{\varphi}^2}{2}$ , in (6) requires a detailed investigation. In [31] it was assumed that  $M(\lambda) = \sigma\lambda$  can be replaced by 0.15 GeV, corresponding to  $\lambda \approx 1 \text{ GeV}^{-1}$ , as it follows from the  $f_\pi, f_K$  calculations, while the  $\varphi\varphi$  Green's function  $G_{\varphi\varphi}(x, y)$ , created by  $\hat{\varphi}^2(x)$  in (6), can be considered nonlocally around the initial and final points  $x$  and  $y$ , which leads to the logarithmically divergent  $G_{\varphi\varphi}(P)$  at the total momentum  $P = (E, 0)$  in the local limit

$$G_{\varphi\varphi}(P) = \frac{1}{(2\pi)^4} \int \frac{d^4p}{(p^2 - m_1^2)((P - p)^2 - m_2^2)}. \quad (7)$$

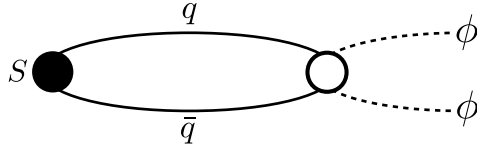


FIG. 3: The scalar  $q\bar{q}$  Green's function with the emission of the chiral mesons

To take into account nonlocality in [31] it was used to cut-off the  $d^3p$  integration at  $|\mathbf{p}| \leq N = 1/\lambda \sim 1 \text{ GeV}$ , implying the nonlocality of the  $(q\bar{q}|\varphi\varphi)$  vertex. Below we shall examine the structure of this nonlocal vertex in more detail, assuming its structure as shown in Fig. 4. As seen, for the distance  $\lambda$  between  $q$  and  $\bar{q}$  (and effectively between  $\varphi$  and  $\varphi$ ) one should have the corresponding Green's functions  $G_{q\bar{q}}$  and  $G_{\varphi\varphi}$  of the form  $G_{q\bar{q}}^{(\lambda)}(x, x'|y, y')$ ,  $G_{\varphi\varphi}^{(\lambda)}(y, y'|u, u')$  with the distance  $\lambda = |\mathbf{x} - \mathbf{x}'| \cong |\mathbf{y} - \mathbf{y}'|$ . The effective value of  $\lambda$  in this vertex  $(q\bar{q}|\varphi\varphi)$  is defined by the product  $G_{q\bar{q}}^{(\lambda)} \sigma \lambda G_{\varphi\varphi}^{(\lambda)}$  and will be found below.

As seen from (6) and following [31], one can find the numerical coefficient  $C_{\varphi\varphi}^{(I)}$  in the transition factor  $k^{(I)}(q\bar{q}|\varphi\varphi)$ , which defines how many  $\varphi\varphi$  are produced by the one  $q\bar{q}$  state. In [31] this was done for isospin  $I = 0, 1$ . Here we shall consider also the case of the  $K\pi$  channel ( $I = 1/2$ ).

We conclude this section with the explicit form of the  $I = 1/2$  isotopic current, producing  $K\pi$  in the case of the  $K_0^*(700)$  resonance.

$$\text{tr} \left( j(u\bar{s}) \frac{\hat{\varphi}^2}{2} \right) = K^+ \frac{\pi^0}{\sqrt{2}} + K^0 \pi^+ \quad (8)$$

$$\text{tr} \left( j(d\bar{s}) \frac{\hat{\varphi}^2}{2} \right) = K^+ \pi^0 - \frac{\pi^0}{\sqrt{2}} K^0 \quad (9)$$

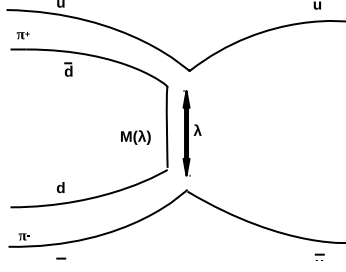


FIG. 4: The transition region  $(q\bar{q}|\varphi\varphi)$  with the spatial distance  $\lambda$  between the constituents

### III. DYNAMICS OF THE $q\bar{q}$ AND THE MESON-MESON SYSTEMS

In this section we analyse the explicit form of the meson-meson  $G_{\varphi\varphi}^{(\lambda)}(yy'|uu')$  and the  $q\bar{q}$  Green's function  $G_{q\bar{q}}^{(\lambda)}(xx'|yy')$ , defined with the initial and final spatial distance  $\lambda$  between  $\varphi$  and  $\varphi$  or  $q$  and  $\bar{q}$ . Since  $G_{q\bar{q}}^{(\lambda)}$  is convergent at  $\lambda = 0$ , we shall consider this effect later in this section and now start with the effect of  $\lambda$  in  $G_{\varphi\varphi}^{(\lambda)}$ , which can be written in the form of the additional factor  $F(\lambda p)$ , appearing in (7), namely,

$$G_{\varphi\varphi}^{(\lambda)}(P) = \frac{1}{(2\pi)^4} \int \frac{d^4 p F(\lambda p)}{(p^2 - m_1^2) ((P - p)^2 - m_2^2)}, \quad (10)$$

where  $F(\lambda p) = \left(\frac{\sin(\lambda p)}{\lambda p}\right)^2$ ,  $p = |\mathbf{p}|$ , is due to averaging over directions of  $\Delta\mathbf{y} = \mathbf{y} - \mathbf{y}'$ ,  $\Delta\mathbf{u} = \mathbf{u} - \mathbf{u}'$ , with  $|\Delta\mathbf{y}| = |\Delta\mathbf{u}| = \lambda$ .

The explicit form of (10) can be written in the c.m. frame

$$\begin{aligned} \text{Re } G_{\varphi\varphi}^{(\lambda)}(E) &= \int_0^\infty \frac{p^2 dp}{4\pi^2} \frac{F(\lambda p)}{\sqrt{p^2 + m_1^2} \sqrt{p^2 + m_2^2}} \times \\ &\times \left\{ \frac{E(\sqrt{p^2 + m_1^2} + \sqrt{p^2 + m_2^2}) + m_1^2 - m_2^2}{[(\sqrt{p^2 + m_1^2} + \sqrt{p^2 + m_2^2})^2 - E^2][E + \sqrt{p^2 + m_1^2} - \sqrt{p^2 + m_2^2}]} \right\} \quad (11) \end{aligned}$$

$$\text{Im } G_{\varphi\varphi}^{(\lambda)}(E) = \frac{F(\lambda p_0)}{16\pi} \frac{\sqrt{[E^2 - (m_1 + m_2)^2][E^2 - (m_1 - m_2)^2]}}{e^2}, \quad (12)$$



where  $p_0$  is found from the relation  $\sqrt{p_0^2 + m_1^2} + \sqrt{p_0^2 + m_2^2} = E \geq m_1 + m$ . Another way of the renormalization of  $\text{Re } G_{\varphi\varphi}(E)$  was accepted in [31], with  $F(\lambda p) \rightarrow 1$  and the fixed upper limit of the  $p$  integration,  $p \leq N = 1/\lambda$ . In what follows we shall compare both ways and find that they produce similar results.

Note, that  $F(\lambda p)$  is actually a function of  $\lambda^2 p^2$ , and therefore it does not contribute to the difference  $G_{\varphi\varphi}^{(\lambda)}(E + i\delta) - G_{\varphi\varphi}^{(\lambda)}(E - i\delta)$  on the cut  $E \geq m_1 + m_2$ , and hence does not violate unitarity condition.

In the case of the  $K\pi$  Green's function one has  $m_1 = m_K$  (493 MeV for  $K^\pm$ ), and  $m_2 = m_\pi \cong 140$  MeV. The resulting form (11) of  $\text{Re } G_{\pi K}^{(\lambda)}(E)$  was computed numerically for  $640 \text{ MeV} \leq E \leq 1200 \text{ MeV}$  for  $\lambda = (0.5; 1; 2; 3) \text{ GeV}^{-1}$

These results show that  $\text{Re } G_{\pi K}^{(\lambda)}(E)$  is almost constant in the range  $[0.64 \div 0, 9]$ . For the following we shall need the values of  $\text{Re } G_{\pi K}^{(\lambda)}$  at  $E = 0.64$  and  $0.8 \text{ GeV}$ , shown in the Table.

TABLE I:

$\lambda$ (GeV <sup>-1</sup> )	$\text{Re } G_{\pi K}^{(\lambda)}$ (640 MeV)	$\text{Re } G_{\pi K}^{(\lambda)}$ (800 MeV)	$\text{Re } G_{\pi K}^{(\lambda)}$ (640 MeV (cut-off))
0.5	0.033	0.028	0.03
1	0.025	0.02	0.022
1.5	0.02	0.0165	0.017
2	0.017	0.013	0.013
3	0.013	0.007	

In the right column of Table 1 the values of  $\text{Re } G_{\pi K}^{(\lambda)}(E = 640 \text{ MeV})$  are obtained in the way as in [31], i.e. with the cut-off of the integral over  $dp$  in (11) at  $N = 1/\lambda$ . One can see rather close values, within (10-15)% accuracy, in the columns 1 and 3, which confirms the cut-off approach used in [31].

Now we shall turn to the  $q\bar{q}$  Green's function and use the same formalism for the  $(n\bar{s})$  system, as in [31] for the  $(n\bar{n})$  system; for that one can exploit the calculated positions of the  $(n\bar{n})$  (see Table II), and analogously the  $(s\bar{s})$ , and  $n\bar{s}$  poles. To calculate the  $q\bar{q}$  Green's function and the  $q\bar{q}$  eigenvalues, we use, as in [31], the exact relativistic formalism, see [43] for a review and references, based on the Field Correlator Method [44]. This yields the relativistic Hamiltonian in the c.m. frame, containing the quark and antiquark kinetic energies  $\omega_1, \omega_2$ ,

$$H(\omega_1, \omega_2, \mathbf{p}) = \sum_{i=1,2} \frac{\mathbf{p} + \omega_i^2 + m_i^2}{2\omega_i} + V_0(r) + V_{s0}(r) + V_T \quad (13)$$

Now one has two options to calculate  $\omega_i$ : 1) to minimize  $H(\omega_1, \omega_2, \mathbf{p})$  in the values of  $\omega_1, \omega_2$ , which leads to the so-called Spinless Salpeter Equation (SSE), widely

used (see e.g. [27]), or to calculate the eigenvalue of (12)  $E(\omega_1, \omega_2)$  and find its minimum (so-called the “einbein approximation” ( $EA$ ), see [28, 30, 43] for details). The comparison of these approximations for the cases of  $n\bar{n}$  scalar meson masses is given in Table II.

The interaction terms  $V_0, V_{s0}, V_T$  are the instantaneous potentials of the scalar confinement  $V_0$ , perturbative and nonperturbative spin-orbit interactions  $V_{s0}$ , and tensor interaction  $V_T$ , which define the center-of-gravity eigenvalue  $M_{\text{cog}}(nP)$ , the spin-orbit correction  $a_{\text{so}}(nP)$ , and the tensor correction  $c_t(nP)$ . For the masses of the  $n^3P_0$  states one has [28, 30]

$$M(n^3P_0) = M_{\text{cog}}(n^3P_0) - 2a_{\text{so}} - c_t. \quad (14)$$

The resulting masses of the  $n\bar{n}$   $n\bar{s}$ ,  $s\bar{s}$  states are given in the Table III

TABLE II: The masses of the  $1^3P_0$  and  $2^3P_0$   $n\bar{n}$  states in MeV, obtained in the SSE, EA and RT (the Regge trajectory formalism) by Badalian and Bakker [28, 30], Ebert et. al. [29] and Godfrey and Isgur [27]

State	BB [28, 30]			EFG [29]	GI [27]
	SSE	EA	RT		
$n\bar{n} 1^3P_0$	1050	1093	1038	1176	1090
$2^3P_0$	1461	1594	1435	1679	1780

As in [31], the lowest pole contribution to the  $(q\bar{q})$  Green’s function  $G_{q\bar{q}}(E)$  can be written as

$$G_{q\bar{q}}(E) = \sum_{n=1}^{\infty} \frac{(f_s^{(n)})^2 M_n^2}{M_n^2 - E^2} = \frac{(f_s^{(1)})^2 M_1^2}{M_1^2 - E^2} + \dots \quad (15)$$

where  $f_s^{(1)}$  is calculated in the  $(n\bar{n})$  case in [31], while for all  $q\bar{q}$  states it is given in Appendix A1, and within 10% of accuracy it has the value,  $f_s^{(1)} \cong 100$  MeV, whereas for the mass  $M_1(n\bar{s})$  one obtains  $M_1 = (1210 \div 1240)$  MeV, and for  $M_1(s\bar{s})$  around 1400 MeV, as it is shown in Table III.

TABLE III: The masses (in MeV) of the  $n^3P_0$  scalars  $q\bar{q}$  obtained in the method of [28, 30] and the experimental resonances in the  $\pi\pi, K\bar{K}, \pi\eta, \pi K$  systems

$n_r$		$n\bar{n}(I=1)$	$n\bar{n}(I=0)$	$n\bar{s}(I=\frac{1}{2})$	$s\bar{s}(I=0)$
0	$M_1$	1.050	1050	1240	1400
	exp	$a_0(980)$	$f_0(980), f_0(500)$	$K_0^*(700)$	$\tilde{f}_0(1370)$
1	$M_2$	1500	1500	1550	1740
	exp	$a_0(1450)$	$f_0(1500)$	$K_0^*(1430)$	$\tilde{f}_0(1710)$

We now can write the final equation for the position of the pole, resulting from the infinite series of the  $(q\bar{q}) \rightarrow (\varphi\varphi) \rightarrow (q\bar{q}) \rightarrow \dots$  transformations in the same way, as it was done in [31].

$$E^2 = M_1^2 \left\{ 1 - k^{(I)}(q\bar{q}|\varphi\varphi) (\text{Re } G_{\varphi\varphi}^{(\lambda)}(E) + i \text{Im } G_{\varphi\varphi}^{(\lambda)}(E)) \right\}, \quad (16)$$

where

$$k^{(I)}(q\bar{q}|\varphi_1\varphi_2) = \frac{C_i^2 M^2(\lambda) (f_s^{(1)})^2}{f_{\varphi_1}^2 f_{\varphi_2}^2}. \quad (17)$$

Here  $C_i^2$  can be found from [31] for the  $\pi\pi, K\bar{K}, \pi\eta$  and from (8), (9) and for  $\pi K$  system it is equal to

$$C_i^2 = \left( 1 + \frac{1}{\sqrt{2}} \right)^2 = \frac{3}{2} + \sqrt{2} = 2.91 \approx 3, \quad (18)$$

while the PS decay constants  $f_i$  are known from [41], experimental and lattice data,

$$f_K = 111 \text{ MeV}, f_\pi = 93 \text{ MeV}, f_\eta = 120 \text{ MeV}. \quad (19)$$

The quark decay constants of the scalar mesons  $f_s^{(i)}$  are calculated via the radial derivative of the  $q\bar{q}$  wave function, as shown in Appendix A1, with the values given in Table VIII. In Appendix A2 it is shown, that  $f_s^{(i)}$  are strongly dependent on the value of  $\lambda$ , and the effective region of  $\lambda$  is inside the range  $0 \leq \lambda \leq 1.5 \text{ GeV}^{-1}$ . At the same time another factor  $M^2(\lambda)$  in (17) grows with  $\lambda$ , so that the optimal values of  $\lambda$  can be obtained from the Table IV, where the ratio  $\frac{k^{(I)}(q\bar{q}|\varphi\varphi)}{k_{\text{max}}^{(I)}(q\bar{q}|\varphi\varphi)} \equiv X(\lambda)$  is given

TABLE IV: The dependence of the ratio of transition factor  $k^I(q\bar{q}|\varphi\varphi)/k_{\text{max}}^{(I)}$  on the spatial contact distance  $\lambda$ .

$\lambda \text{ (GeV)}^{-1}$	0.5	1	1.5	2
$X(\lambda)$	0.29	0.816	1	0.04

As a result, taking into account that  $M(\lambda) = \sigma\lambda = 0.18 \text{ GeV}^2 \cdot \lambda$ , one has the following set of values for the transition factors  $k^{(I)}(q\bar{q}|\varphi\varphi)$  at  $\lambda = 1$  and  $1.5 \text{ GeV}^{-1}$ .

TABLE V: The transition factor  $k^{(I)}(q\bar{q}|\varphi\varphi)$  for different channels at  $\lambda = 1$  and  $1.5 \text{ GeV}^{-1}$

$k(q\bar{q} \varphi\varphi)$	$(n\bar{n} \pi\pi)$	$(n\bar{n} KK)$	$(n\bar{n} \pi\eta)$	$(n\bar{s} \pi K)$	$(s\bar{s} KK)$
$\lambda = 1 \text{ GeV}^{-1}$	18.44	4.02	3.0	14.2	3.0
$\lambda = 1.5 \text{ GeV}^{-1}$	41.51	9.05	6.72	31.2	6.75

Taking these values of  $k^{(I)}(\bar{q}\bar{q}|\varphi\varphi)$  in Eq. (16) and values of  $M_1$  from Table III, one obtains the following resonances in the channels  $\pi\pi, KK, \pi\eta, \pi K$ , given in Table VI.

TABLE VI: The resonances in the channels  $\pi\pi, K\bar{K}, \pi\eta, \pi K$ , coupled at the distance  $1 \text{ GeV}^{-1}$  and  $\lambda = 1.5 \text{ GeV}^{-1}$  to the  $q\bar{q}$  poles ( $n\bar{n}, n\bar{s}, s\bar{s}$ ), in comparison with experimental PDG data

	$(q\bar{q} \varphi\varphi)$	$(n\bar{n} \pi\pi)$	$(n\bar{n} K\bar{K})$	$(n\bar{n} \pi\eta)$	$(n\bar{s} \pi K)$	$(s\bar{s} K\bar{K})$
$\lambda = 1$	$k(q\bar{q} \varphi\varphi)$	18.44	4.02	3.0	14.2	3.0
	$\text{Re } G_{\varphi\varphi}$	0.02	0.011	0.02	0.025	0.011
	$\text{Im } G_{\varphi\varphi}$	0.015	0.02	0.015	0.015	0.02
	$\text{Re } a \text{ Im } a$	0.38;0.276	0.045+i0.08	0.06+i0.045	0.36+ i0.213	0.033+i0.06
	$E$	0.85-i0.17	1.025-i0.044	1.02-i0.025	0.714-i0.078	1.37-i0.041
$\lambda = 1.5$	$k(q\bar{q} \varphi\varphi)$	41.51	9.05	6.75	31.2	6.75
	$\text{Re } G_{\varphi\varphi}$	0.015	0.018	0.018	0.0165	0.018
	$\text{Im } G_{\varphi\varphi}$	0.0155	0.015	0.015	0.015	0.015
	$\text{Re } a \text{ Im } a$	0.645;0.645	0.162+i0.136	0.1215+i0.10	0.52+ i0.468	0.12+i0.10
	$E$	0.64-i0.54	0.966-i0.08	0.98-i0.056	0.75-i0.21	1.31-i0.074
	$E_{PDG}$	0.400-0.550	0.990	0.980	0.630-0.730	1.200-1.500
$\Gamma_{PDG}$	0.400-0.700	0.010-0.100	0.050-0.100	0.478(50)	0.200-0.500	

From Table VI one can see that our pole projection mechanism (PPM) yields a reasonable picture of the resulting resonances in all  $\varphi\varphi$  channels, and the differences between the calculated and observed resonance characteristics ( $R, \Gamma$ ) are of the order of indeterminacy intervals. A possible sign of disagreement seems to be in the  $f_0(500)$  resonance, where PPM gives a resonance position some 150-200 MeV above the experimental value. As it was discussed in [31], this fact implies, that the  $\pi\pi$  interaction in the  $\pi\pi$  Green's function  $G_{\pi\pi}(E)$  is necessary to account for in the low energy region,  $E \lesssim 500 \text{ MeV}$ . Indeed the accurate analysis in [45] confirms the  $f_0(500)$  pole position at  $E = (457 - i279) \text{ MeV}$ , close to  $E_{PDG}$ .

In our case from Table VI for  $\lambda = (1, 1.5) \text{ GeV}^{-1}$  we have

$$E(\text{GeV}) = (0.85 \div 0.64) - i(0.17 \div 0.54), \quad (20)$$

which differs from  $E_{PDG}$ , while  $f_0(980)$  data is comparable to ours.

#### IV. THE CASE OF TWO $q\bar{q}$ POLES

Till now we have considered the lowest  ${}^3P_0$  quark-antiquark poles, which due to the PPM were shifted down from the original position of around (1000–1400) MeV to the final position in the range (700-1300) MeV, which can be associated with the lowest exotic resonances.

However, in the  $(n\bar{n})$  channel there is the radially excited pole  $0^{++}, I = 0$  at the initial position  $M_1 = (1490 - 1500) \text{ MeV}$ , which can be also shifted down and can have the position around 1400 MeV, known as  $f_0(1500)$ . Also in the  $K_0^*$ -channel ( $J^{PC} = 0^{++}, I = \frac{1}{2}$ ) there exists the higher resonance, coupled to the same  $K\pi$  decay channel,  $K_0^*(1430)$ , which can be originated from the radial excited  $(n\bar{s})$  pole

at  $M_2 = 1550$  MeV. Below we shall show a remarkable property of the PPM, where the shift down of the lowest ( $q\bar{q}$ ) pole is almost the same, if the radial excitations are taken into account, while the mass shift of the next ( $q\bar{q}$ ) pole is strongly suppressed as compared to the ground state. This property of the level repulsion follows from the structure of the PPM equations themselves.

Indeed, writing the one-channel, one-pole PPM Eq.(35) in the form as in [31], one has

$$G_{\varphi\varphi}(E)k^{(I)}(q\bar{q}|\varphi\varphi)\frac{M_1^2}{M_1^2 - E^2} = 1, \quad (21)$$

with

$$k^{(I)}(q\bar{q}|\varphi\varphi) = \frac{(C_{\varphi\varphi}^{(I)})^2 M^2(\lambda)(f_s^{(1)})^2}{f_\varphi^4}, \quad f_\varphi = f_\pi, f_K, f_\eta \quad (22)$$

This equation can be generalized, including the radially excited pole  $M_2$ , as follows

$$G_{\varphi\varphi}(E) \left[ k_1^{(I)}(q\bar{q}|\varphi\varphi)\frac{M_1^2}{M_1^2 - E^2} + k_2^{(I)}(q\bar{q}|\varphi\varphi)\frac{M_2^2}{M_2^2 - E^2} \right] = 1 \quad (23)$$

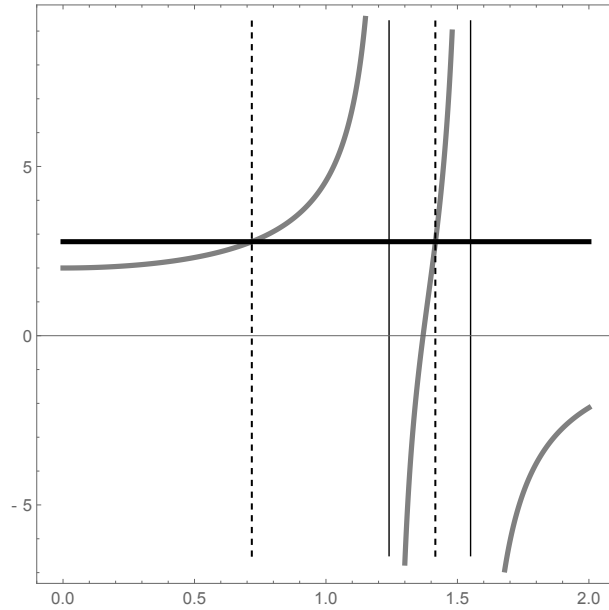


FIG. 5: The function  $f(E)$  vs energy (in GeV) shown by thick grey lines, with two poles at  $E = M_1, M_2$ , shown by thin vertical lines. The intersections of  $f(E)$  with the horizontal line at  $a^{-1} = 1/0.36$  yields two resulting poles  $E = E_1, E_2$ , marked by vertical dashed lines

To understand better the situation with two projected poles we consider the Eq.(23) and approximate  $k_1^{(I)} \approx k_2^{(I)}$  (which holds in most cases according to Table VIII in Appendix A1).

From (23) one has the equation

$$f(E) = \frac{M_1^2}{M_1^2 - E^2} + \frac{M_2^2}{M_2^2 - E^2} = \frac{1}{k^{(I)}G_{\varphi\varphi}(E)} = a^{-1}, \quad (24)$$

Then taking the case  $(n\bar{s}|\pi K)$  as an example and neglecting  $\text{Im } G_{\varphi\varphi}$ , from Table VI one obtains  $a = k^{(1/2)} \text{Re } G_{\pi K} = 0.36$ , and the resulting  $f(E)$  as a function of  $E$  has two poles, given by the intersection of the straight line  $f(E) = \frac{1}{0.36}$ , as shown in Fig. 5. From Fig. 5 one can easily see how the resulting poles  $E_1, E_2$  are shifted as compared to  $M_1, M_2$ , in the approximation of zero  $\text{Im } G_{\pi K}$ .

To proceed with the case of  $K_0^*(700), K_0^*(1430)$ , we are solving the quadratic in  $E^2$  equation(24) with  $M_1 = 1.24, M_2 = 1.55$  GeV, and obtain two approximate solutions for  $\lambda = 1 \text{ GeV}^{-1}$

$$E_1 = (0.78 - i 0.33) \text{ GeV}, \quad E_2 = (1.40 - i 0.035) \text{ GeV}. \quad (25)$$

These solutions correspond to the intersection points in Fig.5, and were obtained treating the imaginary part of  $G_{\pi K}(E)$  as perturbation. To take it fully into account one can write the solution of (24) as

$$E^2 = \frac{1}{2}(M_1^2 + M_2^2)(1 - a) \pm \sqrt{\frac{1}{4}(M_1^2 + M_2^2)^2(1 - a)^2 - M_1^2 M_2^2(1 - 2a)} \quad (26)$$

and use

$$a = \text{Re } a + i \text{Im } a = k^{(I)}(q\bar{q}|\varphi\varphi)(\text{Re } G_{\varphi\varphi} + i \text{Im } G_{\varphi\varphi})$$

from the Table VI for the case  $(n\bar{s}|\pi K)$ , calculated e.g. for  $\lambda = 1 \text{ GeV}^{-1}$ .

In a similar way one can consider all the cases  $(n\bar{n}|\pi\pi), (n\bar{n}|K\bar{K}), (n\bar{n}|\pi\eta), (n\bar{s}|K\pi)$  and  $(s\bar{s}|K\bar{K})$ . The resulting pole positions for  $\lambda = 1 \text{ GeV}^{-1}$ , generated by ground and radially excited scalar  $q\bar{q}$  poles, are given in the Table VII.

One can see in Table VII a reasonable agreement of the predicted and observed resonance characteristics with a few exclusions. The first refers to the higher position of the predicted mass  $f_0(500), E_1 = 800$  MeV, however, with a large width, which implies significant uncertainty in the resonance position, and, as we mentioned above, calls for the account of the  $\pi\pi$  interaction in  $G_{\pi\pi}$  at small energies. The second discrepancy might be more significant. Namely, the first  $(s\bar{s}|K\bar{K})$  resonance occurs exactly at 1.37 GeV (see Table VII) and could be associated with  $f_0(1370)$ , however, the latter prefers to decay into  $\pi\pi, 4\pi$  and the  $K\bar{K}$  ratio is less than 10% [1].

At the same time, the second  $(n\bar{n}|\pi\pi)$  resonance is predicted at around 1.3 GeV with the 100 MeV width  $\Gamma_{\pi\pi}$ , and the  $(n\bar{n}|K\bar{K})$  resonance at 1.45 GeV with the

TABLE VII: Scalar resonances positions and widths in the two-pole formalism

The $(q\bar{q} \varphi\varphi)$ connection	$(n\bar{n} \pi\pi)$	$(n\bar{n} K\bar{K})$	$(n\bar{n} \pi\eta)$	$(n\bar{s} \pi K)$	$(s\bar{s} K\bar{K})$
$n_r = 0$	1.05	1.05	1.05	1.24	1.4
The $q\bar{q}$ mass (GeV)					
$n_1 = 1$	1.50	1.5	1.5	1.55	1.74
Transition coefficient $k^{(I)}(q\bar{q} \varphi\varphi)$	18.44	4.02	3.0	14.2	3.0
$a(E) = k^{(I)}G_{\varphi\varphi}(E)$	0.38+i0.28	0.045+i0.08	0.06+i0.045	0.36+i0.213	0.033+i0.06
$E_1(n_r = 0)$ (GeV),	0.8	1.04	1.02	0.85	1.36
$\Gamma_1$ (MeV)	980	32	40	640	72
	$f_0(500)$	$f_0(980)$	$a_0(980)$	$K_0^*(700)$	$f_0(1370)?$
$E_{PDG}^{(1)}$ (GeV)	0.40-0.55	0.99	0.98	0.63-0.73	1.2 ÷ 1.5
$\Gamma_{PDG}$ (MeV)	400-700	0.10-100	0.50-100	480	200 ÷ 500
$E_2(n_r = 1)$ (GeV)	1.28	1.45	1.45	1.4	1.72
$\Gamma$ (MeV)	100	84	52	40	76
	$f_0(1370)$	$f_0(1500)$	$a_0(1450)$	$K_0^*(1430)$	$f_0(1710)$
$E_{PDG}^{(2)}$	1200-1500	1.50	1.48	1.425	1.72
$\Gamma$ (MeV)	200 ÷ 500	$\Gamma = 109$	$\Gamma = 265$	$\Gamma = 270$	$\Gamma = 120$

width  $\Gamma_{K\bar{K}} \approx 100$  MeV, the latter to be associated with  $f_0(1500)$ . Unfortunately  $f_0(1500)$  does decays mostly into  $\pi\pi, 4\pi$ . Thus one has 3 inconsistencies in the theory:  $\pi\pi$  resonance at 1300 MeV and two  $K\bar{K}$  resonances at 1450 MeV and 1360 MeV, while in experiment one has two resonances  $f_0(1370)$  and  $f_0(1500)$  decaying mostly into  $\pi\pi$  and  $4\pi$ .

Evidently, here appears a strong mixing pattern of three (or more) resonances, which can be additionally enlarged by the code mechanism  $(K\bar{K}|n\bar{n})\frac{M_2}{M_2^* - E^2}(n\bar{n}|\pi\pi)$  near the  $n\bar{n}$  pole at  $M_2 = 1.5$  GeV. As an additional argument for this mixing and the resulting damping of the  $K\bar{K}$  decay mode one can use the small value of the  $K\bar{K}$  decay width of 70 MeV for the  $(s\bar{s}|K\bar{K})$  resonance at 1.36 GeV, while the corresponding experimental resonance  $f_0(1370)$  has a large  $\pi\pi, 4\pi$  width,  $\Gamma = (200 \div 500)$  MeV. This interesting topic requires a substantial analysis and a separate publication.

## V. CONCLUSIONS AND AN OUTLOOK

We have above the simplest version of the channel coupling (CC) mechanism with the two letter code –  $(q\bar{q}|\varphi\varphi)$ , which is the relativistic and chiral extension of the original Cornell code, used for the charmonium resonances in [32]. This is a simple realization of the CC mechanism [35], where an infinite set of transformations of one system into another can provide a pole (bound state) in this set even if both systems are free. The basic role here is played by the magnitude of the transition

amplitude, and a concrete example of the resulting  $Z_b$  resonances was given in the last refs. of [34].

As was demonstrated above, also in the case of scalar mesons the role of transition coefficient  $k^{(I)}(q\bar{q}|\varphi\varphi)$  is very important, since it can be very large ( $k^{(0)}(n\bar{n}|\pi\pi) = O(18 - 40)$ ) in the  $(n\bar{n}|\pi\pi)$  and  $(n\bar{s}|K\pi)$  cases, see Table VI and small ( $k = O(1)$ ) in other cases. One can see in Tables VI and VII, that namely this large range helps to solve the problem of the scalar mesons, where the shift of resonances is so different in different  $\varphi\varphi$  systems, and maximal for the  $(n\bar{n}|\pi\pi)$  case.

Another important feature of our PPM is the appearance of several resonances created by one  $q\bar{q}$  pole – the resulting  $\varphi\varphi$  resonance appears in principle in each  $\varphi\varphi$  system, connected to this  $q\bar{q}$  pole. This happens for  $\pi\pi$  and  $K\bar{K}$  systems, where two resonances  $f_0(500)$  and  $f_0(980)$  are created by the  $q\bar{q}$  pole at  $E = 1050$  MeV. Note, that finally these resonances become connected due to the  $\pi\pi - K\bar{K}$  channel coupling, and in some cases two close-by resonance poles can be located on different sheets, as was observed in lattice analysis by J.Dudek et al. [18].

We have already stressed the important role of the  $\varphi\varphi$  interaction in obtaining the correct position of lowest resonances  $f_0(500)$  and  $K_0^*(700)$ . Actually our approach provides an alternative way for the description of the  $\varphi\varphi$  scattering amplitudes, when the  $q\bar{q}$  dynamics is included at the first stage, and the  $q\bar{q} - \varphi\varphi$  transition is taken into account as a second step, and the final stage should include the detailed account of the  $\varphi\varphi$  interaction. The comparison of the resulting  $\pi\pi$  amplitude, using only two first steps, with the realistic  $\pi\pi$  data, done in [31], exactly shows that the 2-step amplitude roughly describes main features - the extrema and zeros of the amplitude, but strongly distorts the amplitude at small energies, where the  $\varphi\varphi$  interaction is important. To solve the scalar meson problem, as it was demonstrated above, the simplified two-step procedure was sufficient. On another hand, the full 3-step procedure provides the exact  $\varphi\varphi$  amplitude with the correct  $q\bar{q}$  input.

Another feature of the PPM, found in this paper, is the relatively smaller shifts of all radial resonances, compared to the ground states, especially in the  $(n\bar{n}|\pi\pi)$  and  $(n\bar{s}|\pi K)$  cases. As a whole, we have explained the general features of the scalar meson spectrum, leaving the details of the  $K\bar{K} - \pi\pi$  coupling to the future publications.

The work of two of the authors (M.L. and Yu.S.) is supported by the Russian Science Foundation in the framework of the scientific project, Grant 16-12-10414.

## Appendix A1. Decay constants of the $n\bar{n}$ , $n\bar{s}$ and $s\bar{s}$ states



As it was explained in [31], the  $q\bar{q}$  Green's function is computed in the Fock-Schwinger formalism, based on the relativistic path integral method. In this formalism the  $q\bar{q}$  Green's function in the c.m. frame ( $\mathbf{P} = 0$ ) has the form

$$G_{q\bar{q}}(E) = \sum_n \frac{(f_s^{(n)})^2 M_n^2}{M_n^2 - E^2} \rightarrow \frac{(f_s^{(1)})^2 M_1^2}{M_1^2 - E^2} + \frac{(f_s^{(2)})^2 M_2^2}{M_2^2 - E^2}, \quad (\text{A1.1})$$

where  $M_n$ ,  $n = 1, 2$ , are energy eigenvalues, while  $f_s^{(n)}$  are the  $P$ -wave decay constant, which are discussed and calculated in the Appendix 1 of [31].

Here we only detailize the explicit form of  $f_s^{(1)}$  and its dependence on quark masses and the radial quantum number  $n$ .

The explicit form of  $f_s^{(n)}$  can be written as [31]

$$(f_s^{(n)})^2 = \frac{2N_c(R'_{nP}(0))^2}{4\pi\omega_n\bar{\omega}_n M_n}, \quad (\text{A1.2})$$

where  $\omega_n, \bar{\omega}_n$  are the average energies of quark and antiquark in the relativistic  $q\bar{q}$  system obeyed by confinement, color Coulomb and spin-dependent interaction [30]. The concrete calculations, done in this framework as in [31], bring the following results, given in the Table VIII.

TABLE VIII:

$q\bar{q}$	$\omega_1\omega_2$	$R'_{1P}(0)$ GeV <sup>5/2</sup>	$R'_{2P}(0)$ GeV <sup>5/2</sup>	$M_1$ (GeV)	$M_2$ (GeV)	$(f_s^{(1)})^2$ (GeV) <sup>2</sup>	$(f_s^{(2)})^2$ (GeV) <sup>2</sup>
$n\bar{n}$	0.48;0.50	0.0845	0.0906	1.05	1.5	0.0142	0.0103
$n\bar{s}$	0.53;0.56	0.091	0.106	1.24	1.55÷1.61	0.010	0.0108
$s\bar{s}$	0.54;0.50	0.099	0.116	1.4	1.74	0.0112	0.0101

## Appendix A2.

As it is shown in (A1.2), the decay constant  $f_s^{(n)}$  ( $s$ -scalar) is defined via the derivative  $R'_{nP}(0)$ , while other factors in (A1.2) do not depend on  $r$ .

For the decay constant, defined at the spatial distance  $r = \lambda$  between  $q$  and  $\bar{q}$ , as shown in Fig. 4, the decay constant  $f_s^{(n)}(\lambda)$  is determined via the derivative  $R'_{nP}(\lambda)$ , i.e. generalizing Eq.(A1.2),

$$(f_s^{(n)}(\lambda))^2 = \frac{2N_c(R'_{nP}(\lambda))^2}{4\pi\omega_n\bar{\omega}_n M_n} \quad (\text{A2.1})$$

The values of  $R'_{nP}(\lambda)$  have been computed in the relativistic formalism of [28, 30] numerically and the corresponding values of  $R'_{nP}(\lambda), (R'_{nP}(\lambda))^2$  are given in the Table IX together with the ratios of the decay constants  $\left| \frac{f_s(\lambda)}{f_s(0)} \right|^2$

TABLE IX:

$\lambda$ (GeV <sup>-2</sup> )	0.25	0.50	0.75	1.0	1.25	1.50	1.75	2.0
GeV <sup>5/2</sup> $R'_{n,P}(\lambda)$	0.0852	0.082	0.0764	0.0684	0.06	0.0504	0.0101	0.0077
GeV <sup>5</sup> ( $R'_{n,P}(\lambda)$ ) <sup>2</sup>	0.00726	0.00672	0.00583	0.00468	0.0036	0.0025	0.0001	5.9·10 <sup>-5</sup>
$\frac{f_s^{(1)}(\lambda)}{f_s^{(1)}(0)}$	0.98	0.91	0.79	0.63	0.486	0.343	0.0138	0.008

- 
- [1] M. Tanabashi et al., (Particle Data Group) Phys. Rev. **D 98**, 030001 (2018).
- [2] N.Brambilla, S.Eidelman, C.Hanhart, A.Nefediev, C.-P.Shen, C.E.Thomas, A.Vairo and C.-Z.Yuan, arXiv:1907.07583.
- [3] N.A.Törnqvist, Z. Phys. **C68**, 647, (1995), hep-ph/9504372.
- [4] F. E. Close and N. A. Törnqvist, J. Phys. **G 28**, 249 (2002).
- [5] D.V.Bugg, Phys. Rept. **397**, 257 (2004).
- [6] C.Amsler and N.A.Törnqvist, Phys. Rept. **389**, 61 (2004).
- [7] R.L.Jaffe, Phys. Rept. **409**, 1 (2005).
- [8] M.R.Pennington, Int. J. Mod. Phys. **A 21**, 747 (2006), hep-ph/0509265.
- [9] E.Klempt and A.Zaitsev, Phys. Rept. **454**, 1 (2007); arXiv:0708.4016.
- [10] N.N.Achasov, Physics-Uspekhi, **41**, 1149 (1998); Nucl. Phys. (Proc.Suppl.) **A 675**, 279c (2000).
- [11] J.R.Peláez, Phys. Rept. **658**, 1 (2016).
- [12] G.Rupp and E.van Beveren, Acta Phys. Polon. Supp **11**, 455 (2018).
- [13] N.N.Achasov and G.N.Shestakov, Phys. Usp., **62**, 3 (2019).
- [14] R.L.Jaffe, Phys. Rev., **D 15**, 267 (1977); *ibid* **D 15**, 281 (1977); G.'t Hooft, G.Isidori, L.Maiani, A.D.Polosa, and V.Riquer, Phys. Lett. **B 662**, 424 (2008); D.Ebert, R.N.Faustov, and V.O.Galkin, Eur. Phys. J. **C 60**, 273 (2009); G.Eichmann, C.Fischer, and W.Heupel, Phys. Lett. **B 753**, (2016) 282.
- [15] G.Colangelo, J.Gasser, and H.Leutwyler, Nucl. Phys. **B 603**, 125 (2001); I.Caprini, G.Colangelo, H.Leutwyler, Phys. Rev., Lett. **96**, 132001 (2006).
- [16] J.D.Weinstein and N.Isgur, Phys. Rev. Lett., **48**, 659 (1982); Phys. Rev. **D 27**, 588 (1973); *ibid.* **D41**, 2236 (1990); J.A.Oller, E.Oset and A.Ramos, Prog. Part. Nucl. Phys. **45**, 157 (2000); E.Oset et al., Int. J. Mod. Phys. **E 25**, 1630001 (2016); Yu.S.Kalashnikova, and A.V.Nefediev, Phys. Usp. **62**, 568 (2019); arXiv:1811.01324.
- [17] Z. G. Wang, Eur. Phys. J. **C 76**, 427 (2016); arXiv: 1507.02131.
- [18] M. G. Alford and R. L. Jaffe, Nucl. Phys. B **B 578**, 367 (2000), [hep-lat/0001023]; H. Suganuma, K. Tsumura, N. Ishii and F. Okiharu, Prog. Theor. Phys. Suppl. **168**, 168 (2007), arXiv:0707.3309 [hep-lat]; N. Mathur, A. Alexandru, Y. Chen, S. J. Dong, T. Draper, I. Horvath, F. X. Lee, K. F. Liu, S. Tamhankar, and J. B. Zhang, Phys. Rev. **D 76**, 114505 (2007) [hep-ph/0607110]; M. Loan, Z. H. Luo and Y. Y. Lam, arXiv: 0907.3609 [hep-lat]; S. Prelovsek and D.Mohler, Phys. Rev. **D 79**, 014503 (2009); T. Kunihiro, S. Muroya, A. Nakamura, C. Nonaka, M. Sekiguchi, and H. Wada [SCALAR Collaboration], Phys. Rev. D **70**, 034504 (2004), [hep-ph/0310312]; J.J. Dudek, R.G. Edwards, and D.J. Wilson (Hadron Spectrum Collaboration), Phys. Rev.D **93**, 094506 (2016), arXiv:1602.05122 [hep-ph]; D.Darvish, R.Brett, J.Bulava, J.Fallica, A.Hanlon, B.Hörz and C.Morningstar, arXiv:1909.07747.
- [19] E.van Beveren, G. Rupp, EPY, **C 22**, 493 (2001), hep-ex/0106077; Phys. Rev. Lett. **91**, 012003 (2003), hep-ph/0305035; G.Ríos, Phys. Rev. Lett. **97**, 242002 (2006), arXiv:hep-ph/0610397.
- [20] N. N. Achasov and A. V. Kiselev, Phys. Rev. **D 83**, 054008 (2011), *ibid.* **D 85**, 094016 (2012), arXiv:1201.6602; I. Danilkin, O. Deineka and M. Vanderhagen, Phys. Rev. **D 96**, 114018, (2017); I. Danilkin, O. Deineka and M. Vanderhagen, Phys. Rev., arXiv:1909.04158.
- [21] A.V.Anisovich, V.V.Anisovich and A.V.Sarantsev, Phys. Rev. **D 62**, 051502(2000), hep-ph/0003113; J. R. Peláez, J. T. Londergan, J. Nebreda, and A.P.Szczepaniak, Acta Phys. Polon Supp. **7** (2014) 539, arXiv:1404.6058 [hep-ph]; A. V. Anisovich, V.V.Anisovich, M.A.Matveev et al., arXiv:1105.5923.
- [22] E.van Beveren, T. A. Rijken, K.Metzger, C.Dullemond, G.Rupp, and Y. E. Ribeiro, Z.Phys. **C 30**, 615 (1986), arXiv:0710.4067 [hep-ph].
- [23] N. A. Tornqvist and M.Roos, Phys. Rev. Lett. **76**, 1575 (1996), arXiv:hep-ph/9511210.
- [24] M. Boggione and M. R. Pennington, Phys. Rev. **D 65**, 114010 (2002), arXiv:hep-ph/0203149 [hep-ph].
- [25] T. Wolkanowski, F. Giacosa, and D. H. Rischke, Phys. Rev. **D 93**, 014002 (2016), arXiv:1508.00372 [hep-ph].
- [26] I. K. Hammer, C.Hanhart and A.V.Nefediev, Eur. Phys. J. **A 52**, (2016) 330, arXiv:1607.06971.
- [27] S.Godfrey and N.Isgur, Phys. Rev. **D32**, 189 (1988).
- [28] A.M.Badalian and B.L.G.Bakker, Phys. Rev. **D 67** 071901 (2003).
- [29] D.Ebert, R.N.Faustov and V.O.Galkin, Phys. Rev. **D 79**, 114029 (2009), arXiv:0903.5183.
- [30] A.M.Badalian and B.L.G.Bakker, Phys. Rev. **D 100** 034010 (2019), arXiv:1901.10280.
- [31] M.S.Lukashov and Yu.A.Simonov, arXiv: 1909.10384.

- [32] E.Eichten, K.Gottfried, K.Kinoshita, K.D.Lane and T.M.Yan, Phys.Rev. **D 17**, 3090 (1978); E.Eichten, K.Gottfried, K.Kinoshita, K.D.Lane and T.M.Yan, Phys.Rev. **D 21**, 203 (1980).
- [33] E.Eichten, K.Lane and C.Quigg, Phys.Rev. **D 69**, 094019 (2004), hep-ph/0401210; Yu.S.Kalashnikova, Phys.Rev. **D72**, 034010 (2005).
- [34] I.V.Danilkin and Yu.A.Simonov, Phys. Rev. **D 81**, 074027 (2010), arXiv:0907.1088; I.V.Danilkin and Yu.A.Simonov, Phys. Rev. Lett. **105**, 102002 (2010), arXiv:1006.0211; I.V.Danilkin, V.D.Orlovsky and Yu.A.Simonov, Phys. Rev. **D 85**, 0340 (2012), arXiv:1106.1552.
- [35] A. M. Badalian, L.P.Kok, M.I.Polikarpov and Yu.A.Simonov, Phys. Rept.**82**, 31 (1982).
- [36] Yu.A.Simonov, Phys. Rev. **D 65**, 094018 (2002) hep-ph/0201170.
- [37] Yu.A.Simonov, Phys. Atom. Nucl. **67**, 846 (2004); hep-ph/0302090.
- [38] Yu.A.Simonov, Phys. Atom. Nucl. **67**, 1027 (2004); hep-ph/0305281.
- [39] Yu. A. Simonov, Int. J. Mod. Phys. **A 31**, 1650104 (2016), arXiv: 1509.06930.
- [40] M.Gell-Mann, R.L.Oakes and B.Renner, Phys Rev. **175**, 2195 (1968).
- [41] Yu. A. Simonov, Phys. Atom. Nucl. **79**, 265 (2016), arXiv:1502.07569.
- [42] M.A.Andreichikov and Yu.A.Simonov, Eur. Phys. J. **C 78**, 902 (2018), arXiv:1805.11896.
- [43] Yu.A.Simonov, Phys. Rev. **D 99**, 096025 (2019), arXiv:1902.05364.
- [44] Yu.A.Simonov, Phys. Rev., **D 99** 056012 (2019), arXiv:1804.08946;  
A. Di Giacomo, H. G. Dosch, V. I. Shevchenko, and Yu. A. Simonov, Phys. Rept. **372**, 319 (2002); H.G.Dosh and Yu.A.Simonov, Phys. Lett. **B 205** , 339 (1988).
- [45] R.Garcia-Martin, R.Kaminski, J.K.Peláez et al., Phys. Rev. Lett. **107**, 072001 (2011); J.K.Peláez, A.Rodas and J.Kuiz De Elvira, Eur. Phys. J. **C 79**, 1008 (2019).